

# Tuning of magnetic ground state of the spin- $\frac{1}{2}$ square-lattice compound $\text{Zn}_2\text{VO}(\text{PO}_4)_2$ through chemical substitution

Sudipta Kanungo, Satyaki Kar, and T. Saha-Dasgupta

*S. N. Bose National Centre for Basic Sciences, Kolkata, India*

(Received 20 December 2012; revised manuscript received 2 February 2013; published 25 February 2013)

Using first-principles density-functional-theory-based calculations, we derive the low-energy spin model of the compound  $\text{Zn}_2\text{VO}(\text{PO}_4)_2$ , and  $\frac{1}{4}$ th Ti-substituted compound  $\text{Zn}_8\text{TiV}_3\text{O}_4(\text{PO}_4)_8$  which is yet to be synthesized. We compute the thermodynamics properties of the proposed spin models by the quantum Monte Carlo technique. For the pristine compound  $\text{Zn}_2\text{VO}(\text{PO}_4)_2$  our computed susceptibility is found to be in good agreement with the available experimental data and is in accordance with the earlier proposed spin model of the spin- $\frac{1}{2}$  antiferromagnetic square lattice. Upon Ti substitution, which may be viewed as  $\frac{1}{4}$ -spin depletion, the two-dimensional antiferromagnetic square-lattice behavior of the parent compound is found to be altered significantly, giving rise to spin-gap behavior. We hope that our work will stimulate further experimental studies on this compound.

DOI: [10.1103/PhysRevB.87.054431](https://doi.org/10.1103/PhysRevB.87.054431)

PACS number(s): 75.10.Jm, 75.30.Et, 71.20.-b

## I. INTRODUCTION

Transition-metal-oxide (TMO)-based low-dimensional quantum spin systems (QSS) form an active area of research in condensed matter physics. The study of such systems are of interest due to the presence of a quantum fluctuation driven ground state showing unusual low-temperature properties.<sup>1</sup> A pertinent question in this area of study remains: Given a compound, what is the underlying spin model? Often the spin model, derived based on structural details of the compound, turns out to be inaccurate. The interactions connecting magnetic sites depend on the positions of the intervening ligands and the hybridization of the ligand  $p$  orbital with the transition metal  $d$  orbital, which also needs to be taken into consideration. A famous example in this context is that of  $(\text{VO})_2\text{P}_2\text{O}_7$ , which turns out to be an alternating spin chain compound<sup>2</sup> while originally it was thought of as a two-leg spin ladder system based on structural considerations.<sup>3</sup> The literature on first-principles calculations for the microscopic understanding of the appropriate spin model for given compounds is, therefore, growing.<sup>4</sup>

An interesting aspect of the study of QSS is the exploration of emergent phenomena by perturbing the system via the external tunable parameter, once the understanding of the ground state of the unperturbed system is achieved. Besides temperature, the available external tuning parameters include magnetic field,<sup>5-7</sup> and hydrostatic and uniaxial pressure.<sup>8-11</sup> The other alternative route can be to chemically perturb the system via magnetic or nonmagnetic ion substitution.<sup>12-17</sup>

In the present study we carry out first-principles density-functional-theory (DFT)-based calculations combined with quantum Monte Carlo calculations to characterize the underlying spin model and the thermodynamic properties of  $\text{Zn}_2\text{VO}(\text{PO}_4)_2$  which has been designated a spin- $\frac{1}{2}$  Heisenberg antiferromagnetic (HAF) square lattice based on magnetic susceptibility and neutron diffraction experiments.<sup>18,19</sup> Our study finds good agreement with the conclusion drawn from the experimental measurements.<sup>18,19</sup>  $\text{Zn}_2\text{VO}(\text{PO}_4)_2$ , characterized as the spin- $\frac{1}{2}$  HAF square-lattice system, exhibits long-ranged magnetic ordering.<sup>18,19</sup> The stability of the long-ranged ordered ground state in such a type of system has been

the focus of attention. In particular, the depletion of spins in destabilization of long-range order has been studied. For example, spin ladder compounds were obtained by breaking the planes of copper oxide materials.<sup>20</sup> Depletion of  $\frac{1}{4}$ -spins in a triangular antiferromagnetic Heisenberg lattice leads to formation of the kagome lattice.<sup>21</sup> By depletion, bonds between spin are weakened, thereby enhancing the importance of quantum fluctuation which may destroy the long-range ordering opening up a finite spin gap. This has been observed in the case of the  $\text{CaV}_4\text{O}_9$  compound,<sup>22</sup> which has been shown as  $\frac{1}{5}$ -depleted two-dimensional (2D)  $S=\frac{1}{2}$  Heisenberg AF. Following such ideas, we explored the chemical route of tuning the ground state of  $\text{Zn}_2\text{VO}(\text{PO}_4)_2$ , by the substitution of one magnetic V ion by the nonmagnetic Ti ion out of four V ions. This would lead to the  $\frac{1}{4}$ -spin depleted situation. We choose  $\frac{1}{4}$ -substitution which is the simplest possible substitution with one missing spin in each plaquette of four nearest neighbor V spins. We predict a destabilization of the long-range ordered ground state of  $\text{Zn}_2\text{VO}(\text{PO}_4)_2$  upon Ti substitution, showing a spin-gap behavior. This establishes the tuning of the ground-state properties via the chemical route. Our theoretical prediction can be checked through future experiments.

## II. METHODOLOGY

The DFT calculations were carried out using two different basis sets: (a) the MTO-based linear muffin tin orbital (LMTO)<sup>23</sup> and its  $N$ th order extension<sup>24</sup> NMTO method as implemented in Stuttgart code<sup>25</sup> and (b) plane-wave-based pseudopotential framework as implemented in the VIENNA *ab initio* simulation package (VASP).<sup>26</sup> The exchange correlation function was chosen to be that of generalized gradient approximation (GGA) implemented following the Perdew-Burke-Ernzerhof prescription.<sup>27</sup> In the structural optimization, we replace one V atom out of 4 V atoms in a supercell and we optimize the atomic positions as well as the lattice constants. The position of the atoms were relaxed towards equilibrium until the Hellman-Feynman force became less than 0.01 eV/Å. For the plane-wave calculation, a 600-eV plane-wave cutoff

was used. A  $k$ -point mesh of  $6 \times 6 \times 8$  in the Brillouin zone was used for self-consistent calculations. The construction of the low-energy Hamiltonian in the first-principles-derived Wannier function basis has been achieved through the NMTO-downfolding technique.<sup>24</sup> Starting from a full DFT calculation, NMTO-downfolding arrives at a few-orbital Hamiltonian by integrating out degrees which are not of interest. It does so by defining energy-selected, effective orbitals which serve as Wannier-like orbitals defining the few-orbital Hamiltonian in the downfolded representation. The method provides a first-principles way for deriving a few-band, tight-binding Hamiltonian of the form  $H_{\text{TB}} = \sum_{ij} t_{ij}^{m,m'} (c_{i,m}^\dagger c_{j,m'} + \text{H.c.})$  for a complex system, where the  $t_{ij}^{m,m'}$  define the effective hopping between the active, nondownfolded orbitals,  $m$  and  $m'$ .  $c_{i,m}^\dagger$  ( $c_{i,m}$ ) are electron creation (annihilation) operators on site  $i$  at orbital  $m$ . The NMTO technique which is not yet available in its self-consistent form relies on the self-consistent potential parameters obtained out of linear muffin-tine orbital (LMTO)<sup>23</sup> calculations. The results were cross-checked among the plane wave and LMTO calculations in terms of total energy differences, density of states, and band structures. The missing correlation effect beyond GGA is taken into account through GGA +  $U$  calculations.<sup>28</sup>

### III. CRYSTAL STRUCTURE

$\text{Zn}_2\text{VO}(\text{PO}_4)_2$  form in the tetragonal crystal structure<sup>29</sup> of space group  $I4cm$  with lattice parameters,  $a = 8.93 \text{ \AA}$ ,  $c = 9.04 \text{ \AA}$ , and with two formula units in the unit cell. The basic units forming the structure are  $\text{VO}_5$  square pyramids,  $\text{ZnO}_5$  square pyramids, and  $\text{PO}_4$  tetrahedra as shown in Figs. 1(a), 1(b), and 1(c) respectively. Within the  $ab$  layer the nearest neighbor ( $NN$ )  $\text{VO}_5$  pyramids are connected via corner sharing  $\text{PO}_4$  tetrahedral units while the next  $NN$   $\text{VO}_5$  are connected by two  $\text{ZnO}_5$  pyramids which edge share with each other as shown in Fig. 1(d).  $\text{VO}_5$  and  $\text{PO}_4$  units point in the same direction while  $\text{ZnO}_5$  points in the opposite direction. Different

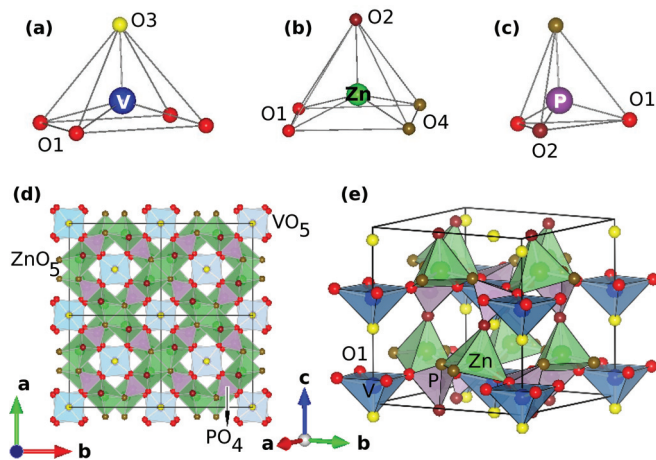


FIG. 1. (Color online) (a)–(c)  $\text{VO}_5$ ,  $\text{ZnO}_5$ , and  $\text{PO}_4$  structural units. The larger ball represents either V or Zn or P while the smaller balls represent O. Various inequivalent O atoms have been marked. (d) The projection of the structure in the  $ab$  plane, showing the square planar arrangement of  $\text{VO}_5$  pyramids. (e) The three-dimensional connected structure.

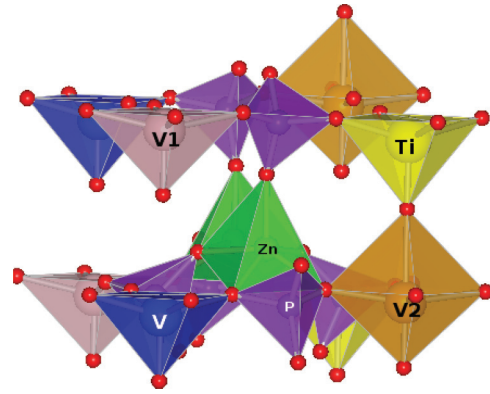


FIG. 2. (Color online) The crystal structure of  $\frac{1}{4}$ -Ti substituted  $\text{Zn}_2\text{VO}(\text{PO}_4)_2$ .

layers are stacked above each other along the crystallographic  $c$  direction and they are connected via corner shared  $\text{ZnO}_5$  and  $\text{PO}_4$  units, giving rise to the three-dimensional (3D) connected network as shown in Fig. 1(e). Substituting one V atom by Ti out of four V atoms in a  $1 \times 1 \times 2$  supercell, as shown in Fig. 2, lowers the tetragonal  $I4cm$  symmetry to monoclinic  $A2$  symmetry<sup>30</sup> with  $a = 12.851 \text{ \AA}$ ,  $b = 9.180 \text{ \AA}$ ,  $c = 12.852 \text{ \AA}$ , and  $\beta = 90.02^\circ$ , and giving rise to the three nonequivalent class of V atoms: V, V1, and V2 (see Fig. 2). V1 is neighbor to Ti within the plane, V2 is neighbor to Ti both in plane and along the out-of-plane direction while V does not have any Ti as neighbor. For V1, this gave rise to two V neighbors along one of the in-plane directions and two V neighbors in the out-of-plane direction. For V, there are two V2 and two V1 neighbors along two in-plane directions and two V1 neighbors in the out-of-plane direction. For the V2 atom, on the other hand, there are only two V neighbors along one of the in-plane directions and no out-of-plane vanadium neighbor. The degeneracy of Zn, P, and various O atoms are also additionally lifted. The crystal structure data of Ti-substituted  $\text{Zn}_2\text{VO}(\text{PO}_4)_2$  in comparison to pristine  $\text{Zn}_2\text{VO}(\text{PO}_4)_2$ , obtained through complete structural relaxation, is shown in Table I. The important structural parameters like V-O bond lengths and O-V-O bond angles are shown in Table II. We find that Ti substitution brings in further distortion in the  $\text{VO}_5$  pyramidal unit, in the sense that while the  $\text{VO}_5$  pyramids in the pristine compound are regular square pyramids with all V-O bond lengths in the basal plane being equal and with short V-O apical bond, for the Ti-substituted compound the V-O bond lengths even in basal plane become unequal.

### IV. ELECTRONIC STRUCTURE

The nonspin polarized GGA density of states (DOS) of the pristine compound, as shown in Fig. 3, consist of  $d$ - $p$  hybridized states ranging from about 6 eV below the Fermi level ( $E_F$ ) to about 4 eV above  $E_F$ . The states below  $-4 \text{ eV}$  or so are dominated by O- $p$  states, while the states close to  $E_F$  or above  $E_F$  (within the range of plot) is dominated by the V- $d$  states. The square pyramidal crystal field around the V atoms splits the V- $d$  states into low-lying V- $d_{xy}$  states which are separated by a large energy gap of  $\approx 1 \text{ eV}$  from the other  $d$  states. The energy level splitting of  $d$  states at V sites

TABLE I. Various atomic positions of the pristine  $\text{Zn}_2\text{VO}(\text{PO}_4)_2$  and Ti-substituted  $\text{Zn}_8\text{TiV}_3\text{O}_4(\text{PO}_4)_8$  compounds.

Atom	Pristine compound			Atom	Ti-doped		
	x	y	z		x	y	z
Zn	0.618	0.118	0.264	Zn1	0.247	0.235	-.129
V	0.000	0.000	0.101	Zn2	0.131	0.237	0.249
P	0.307	0.193	0.120	Zn3	0.250	-.265	0.133
O1	0.827	0.135	0.155	Zn4	0.367	0.233	0.252
O2	0.652	0.152	0.469	V	0.000	-.095	0.000
O3	0.000	0.000	0.427	V1	0.000	0.384	0.000
O4	0.396	0.104	0.237	V2	0.500	-.141	0.000
				Ti	0.500	0.418	0.000
				P1	0.249	-.121	-.055
				P2	0.057	-.119	0.250
				P3	0.249	0.382	0.059
				P4	0.442	-.121	0.249
				O1	0.000	0.083	0.000
				O2	0.152	-.150	0.016
				O3	-.016	-.147	0.154
				O4	0.257	0.033	-.094
				O5	0.099	0.033	0.255
				O6	0.156	0.341	-.017
				O7	0.017	0.342	0.156
				O8	0.000	-.439	0.000
				O9	0.247	-.232	-.147
				O10	0.146	-.234	0.249
				O11	0.253	0.263	0.146
				O12	0.340	-.167	0.019
				O13	0.346	0.361	-.014
				O14	0.239	0.031	-.394
				O15	0.399	0.030	0.237
				O16	0.353	-.236	0.255
				O17	0.500	0.035	0.000
				O18	0.482	-.167	-.159
				O19	0.500	-.393	0.000
				O20	0.486	-.141	-.348

obtained by NMTO calculation of keeping  $V-d$  states active and downfolding the rest and considering the onsite block of the real space Hamiltonian in the downfolded  $V-d$  basis is shown in the upper inset of Fig. 3. V atom in  $\text{Zn}_2\text{VO}(\text{PO}_4)_2$  is in nominal  $4+$  states with  $d^1$  occupancy. Half filled  $V-d_{xy}$  states therefore cross the Fermi level as shown in the band structure plot of Fig. 4(a), which hybridizes with the  $O-p$  and  $P-p$  states as shown in the lower inset in Fig. 3. Inclusion of the correlation effect beyond GGA in the half filled  $V-d_{xy}$  gives rise to the insulating solution through formation of lower and upper Hubbard bands, as has been checked through GGA + U calculations.<sup>28</sup> The low energy Hamiltonian of the system thus can be constructed in terms of  $V-d_{xy}$  only model. In order to construct the low energy Hamiltonian of the system in an *ab initio* way, we carried out NMTO downfolding calculation, in which the only  $V-d_{xy}$  degrees of freedom were kept active and all the rest, including other  $V-d$  states, were downfolded. The downfolded  $V-d_{xy}$  band in comparison to the full band is shown in Fig. 4(b). This process led to construction of the effective  $V-d_{xy}$  Wannier function which has the central part shaped according to  $V-d_{xy}$  symmetry and tails shaped according to integrated out degrees of freedom, admixing with  $V-d_{xy}$  char-

TABLE II. The TM-O bond lengths and O-TM-O bond angles in pristine  $[\text{Zn}_2\text{VO}(\text{PO}_4)_2]$  and Ti-substituted  $[\text{Zn}_8\text{TiV}_3\text{O}_4(\text{PO}_4)_8]$  compounds.

Unit	Pristine compound	Ti-substituted
$\text{VO}_5$	V-O(basal) = 2.01Å	V-O(basal) = 1.99Å 2.11Å
	V-O(apical) = 1.56Å	V-O(apical) = 1.63Å
	O-V-O(basal) = 86.7°	O-V-O(basal) = 86.1° 86.6°
	O-V-O(apical) = 103.9°	O-V-O(apical) = 104.3° 105.1°
		V1-O(basal) = 2.02Å 2.02Å
		V1-O(apical) = 1.62Å
		O-V1-O(basal) = 87.0° 87.4°
		O-V1-O(apical) = 102.6° 102.8°
		V2-O(basal) = 2.03Å 2.03Å
		V2-O(apical) = 1.62Å
$\text{TiO}_5$		O-V2-O(basal) = 88.6° 88.9°
		O-V2-O(apical) = 98.2° 98.4°
		Ti-O(basal) = 2.03Å 2.01Å
		Ti-O(apical) = 1.71Å
		O-Ti-O(basal) = 85.6° 85.8°
		O-Ti-O(apical) = 105.5° 106.2°

acter, as shown in Fig. 4(c). The real space Hamiltonian defined in the basis of the effective  $V-d_{xy}$  Wannier function provides estimates of various V-V effective hopping interactions which are listed in Table III. The various dominant hoppings are shown in Fig. 5. The strongest hopping interaction turns out to be in plane  $NN$  interaction ( $t_1$ ), connecting two V atoms at the center and corner of the square in the  $ab$  plane. The out of plane V-V distance though shorter than that of in-plane V-V distances, the corresponding hopping interaction ( $t_c$ ) is found to be about a factor of 8 weaker compared to the strongest in-plane hopping interaction ( $t_1$ ). The V-V hopping along the edge of the square ( $t_2$ ) is also weak, about a factor of 7 weaker compared to  $t_1$ . Our study therefore confirms  $\text{Zn}_2\text{VO}(\text{PO}_4)_2$  should be described as a weakly coupled square-lattice system rather than a chain system which was proposed<sup>29</sup> based solely on the structural consideration. The super-exchange path corresponding to the strongest interaction is shown in Fig. 4(c) as the overlap of two effective  $V-d_{xy}$  Wannier functions at two  $NN$  in plane V sites. We find that  $O-p$ -like tails of the Wannier function bend toward the intervening P sites indicating the importance of the hybridization effect from the P atom. This is justified by finite nonzero contribution of  $P-p$  projected DOS in the energy range of  $V-d_{xy}$  dominated DOS as is shown in the lower inset of Fig. 3. The strongest V-V interaction is therefore mediated by the V-O-P-O-V super-super-exchange

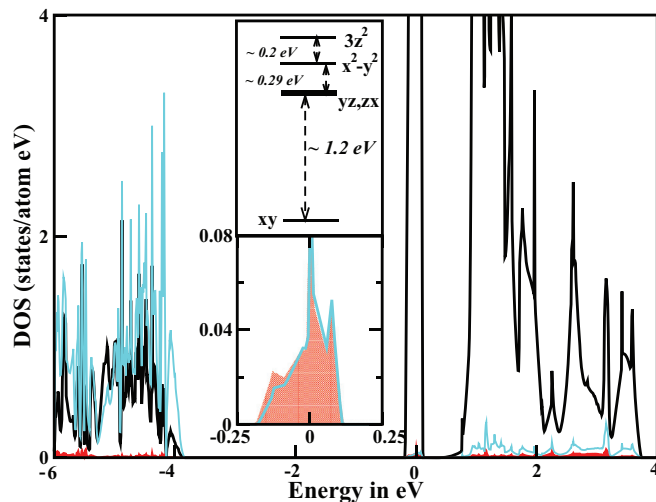


FIG. 3. (Color online) Non-spin-polarized density of states of  $\text{Zn}_2\text{VO}(\text{PO}_4)_2$  as obtained in GGA calculation. The zero of the energy is set at GGA Fermi energy. The black solid line, cyan (gray) solid line, and the shaded area represent the density of states projected onto  $V-d$ ,  $O-p$ , and  $P-p$ , respectively. The upper inset shows the energy level positions of the  $V-d$  level as obtained in NMTO downfolding calculation. The lower inset shows the zoomed plot showing the contribution of the  $O-p$  and  $P-p$  states to the  $V-d_{xy}$  derived states that cross the Fermi energy.

path similar to that found in  $(\text{VO})_2\text{P}_2\text{O}_7$ .<sup>31</sup> In the limit of large correlation, typically valid for transition to the metal-oxide-

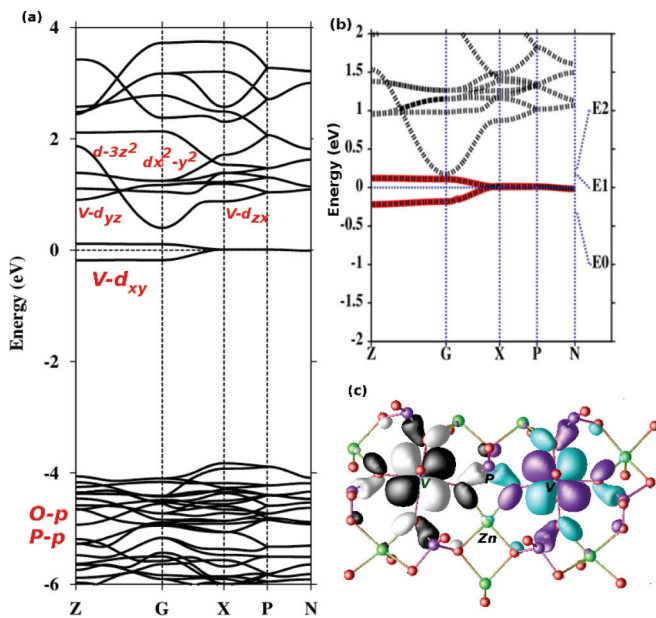


FIG. 4. (Color online) (a) The band structure of  $\text{Zn}_2\text{VO}(\text{PO}_4)_2$  plotted along the high symmetry points of the tetragonal Brillouin zone. The dominant orbital characters of the bands have been marked. (b) The downfolded  $V-d_{xy}$  band (fat solid line) in comparison to full band structure (dashed line). The energy points indicate the energies about which the expansion has been made in NMTO downfolding calculation. (c) The overlap of  $V-d_{xy}$  Wannier functions placed at two  $NN$ ,  $V$  sites in the  $ab$  plane. Shown are the constant value surfaces with positive and negative lobes colored differently.

TABLE III. Dominant hopping interactions for the pristine and Ti-substituted compounds. Hopping interactions less than 1 meV have been neglected.

Pristine compound			Ti-substituted compound		
Dist.	No. of neighbors	Hopping	Dist.	No. of neighbors	Hopping
4.51 Å	2	5.20 meV ( $t_c$ )	4.64 Å	1	6.00 meV ( $t'_c$ )
6.30 Å	4	39.7 meV ( $t_1$ )	6.31 Å	2	39.7 meV ( $t'_1$ )
8.92 Å	4	6.80 meV ( $t_2$ )	6.32 Å	2	9.50 meV ( $t'_1$ )

based system, the antiferromagnetic exchange interaction  $J$  is related to the hopping integral  $t$ , obtained in a single-particle theory, by second-order perturbation relation  $J = 4t^2/U$ ,  $U$  being the effective onsite Coulomb repulsion. The effective hopping strengths, therefore, already provide a good idea of the underlying spin model, giving rise to information of relevant super-exchange paths. To obtain a more accurate estimate of the magnetic interactions as well as to take into account the ferromagnetic contribution of the exchange interaction, we carried out total energy calculations within GGA +  $U$  with a choice of  $U = 4$  eV and  $J_H = 1$  eV for different arrangements of  $V$  spins, and mapped onto the energetics of the corresponding Heisenberg model. Such an approach is found to be highly successful in the description of spin models and in providing estimates of magnetic interactions in a number of cases.<sup>32</sup> This gave rise to antiferromagnetic  $J_1$  of magnitude 10 K,  $J_2/J_1 = 0.02$  and  $J_3/J_1 = -0.03$ , in good agreement with the values obtained by fitting the susceptibility data<sup>18</sup> and neutron scattering data.<sup>19</sup>

Upon substitution of Ti, in one  $V$  site out of four  $V$  sites in a  $1 \times 1 \times 2$  supercell, the band structure changes significantly. In the upper panels of Fig. 6, we show the GGA band structure of pristine and  $\frac{1}{4}$ -Ti-substituted compound, both plotted for the  $1 \times 1 \times 2$  supercell. The  $1 \times 1 \times 2$  supercell of  $\text{Zn}_2\text{VO}(\text{PO}_4)_2$  contains four  $V$  sites giving rise to the four  $V-d_{xy}$  bands which cross the Fermi energy. Upon Ti substitution, Ti- $d_{xy}$  band which is empty splits off from the manifold of the  $V-d_{xy}$  band with a gap of about 0.5 eV and remains dispersionless. The three  $V$  atoms which have become inequivalent due to Ti substitution, give rise to three  $V-d_{xy}$  band crossing Fermi levels, in accordance with their half-filled nature. The degeneracy of bands getting lifted at several  $k$  points is compared to the band structure of the pristine

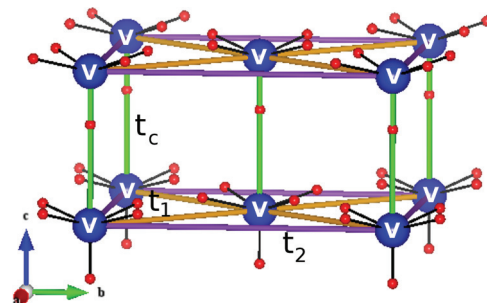


FIG. 5. (Color online) The  $V$  only sublattice of  $\text{Zn}_2\text{VO}(\text{PO}_4)_2$ . Shown are the dominant hoppings,  $t_1$ ,  $t_2$ , and  $t_c$ .

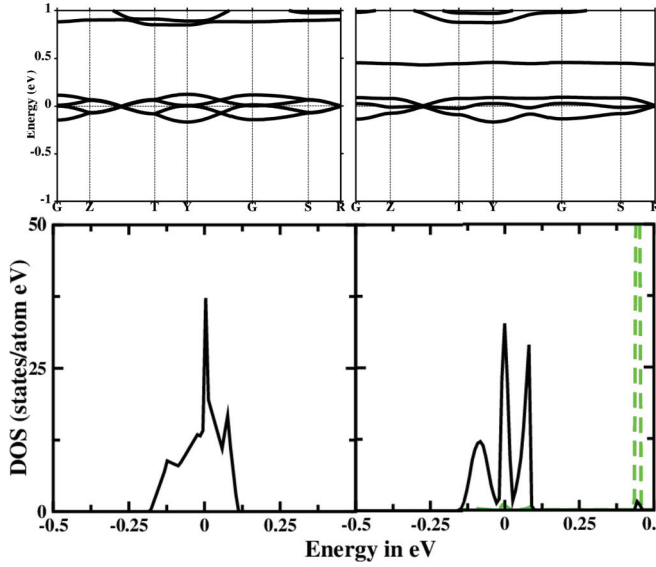


FIG. 6. (Color online) (Upper panels) Comparison of the band structure of  $\text{Zn}_2\text{VO}(\text{PO}_4)_2$  (left panel) and  $\text{Zn}_8\text{TiV}_3\text{O}_4(\text{PO}_4)_8$  (right panel) plotted along the high symmetry points of the supercell. (Lower panel) The density of states of  $\text{Zn}_2\text{VO}(\text{PO}_4)_2$  (left panel) and  $\text{Zn}_8\text{TiV}_3\text{O}_4(\text{PO}_4)_8$  (right panel). The V- $d$  and Ti- $d$  (applicable for the right panel) projected states are shown as solid and dashed lines.

compound due to the breaking of degeneracy between different V atoms. Comparing the DOS of the two compounds as shown in the lower panels of Fig. 6, we find that widths of the V- $d_{xy}$  dominated states are nearly the same in two cases, indicating strengths of the strongest V-V interaction to be nearly the same. Carrying out the NMTO-downfolding calculation to define the effective V- $d_{xy}$  low-energy Hamiltonian, as done for the pristine compound and constructing the real space Hamiltonian, we find the dominant hopping interactions which are listed in Table III. Comparing with the interactions of the pristine compound, we find that four  $NV$  in-plane interactions ( $t_1$ ) which were strongest for the pristine compound, group into two strong (connecting V and V1)  $t'_1$  and two weak (connecting V and V2)  $t''_1$  interactions.

Similarly, the out-of-plane interaction is significant only for the interaction from V to V1, and not the other way, which makes a pair of out-of-plane connected V atoms for  $\text{Zn}_8\text{TiV}_3\text{O}_4(\text{PO}_4)_8$  rather than a chain of V atoms connected in the out-of-plane direction as in the case of  $\text{Zn}_2\text{VO}(\text{PO}_4)_2$ . The total energy GGA + U calculation to estimate the strengths of magnetic interactions corresponding to  $t'_1$ ,  $t''_1$ , and  $t'_c$  gave rise to values  $J'_1 = 8$  K,  $\frac{J''_1}{J'_1} = 0.03$ , and  $\frac{J'_c}{J'_1} = -0.04$ . The spin model for pristine and  $\frac{1}{4}$ -Ti-substituted compounds, therefore, can be described as the weakly coupled 2D, AFM square lattice and the weakly coupled one-dimensional (1D) AFM chain, respectively, as shown in Fig. 7.

## V. CALCULATION OF MAGNETIC PROPERTIES

In the next step we computed the magnetic susceptibility as well as magnetization properties by considering the spin- $\frac{1}{2}$  Heisenberg model on  $N_1 \times N_2 \times N_3$  lattices. The description of spin models for the pristine and Ti-substituted compounds

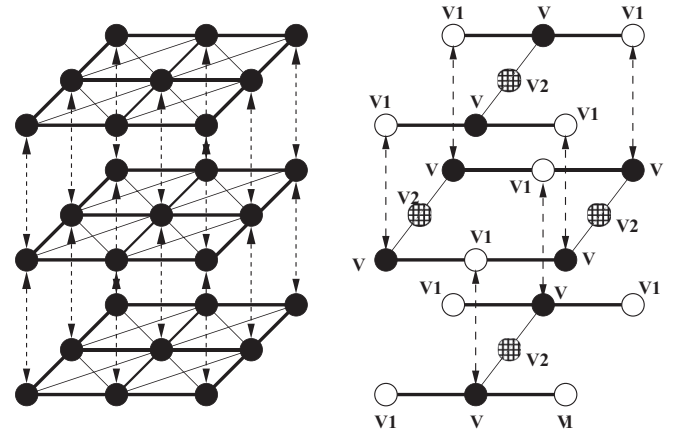


FIG. 7. The spin models corresponding to  $\text{Zn}_2\text{VO}(\text{PO}_4)_2$  (left panel) and  $\text{Zn}_8\text{TiV}_3\text{O}_4(\text{PO}_4)_8$  (right panel) compounds. The thick solid, thin solid, and dashed lines represent strongest  $J_1$  ( $J'_1$ ) and weak  $J_2$  ( $J''_1$ ) and  $J_c$  ( $J'_c$ ) interactions for the  $\text{Zn}_2\text{VO}(\text{PO}_4)_2$  [ $\text{Zn}_8\text{TiV}_3\text{O}_4(\text{PO}_4)_8$ ] compound. The spins corresponding to inequivalent V ions in the case of the substituted  $\text{Zn}_8\text{TiV}_3\text{O}_4(\text{PO}_4)_8$  compound has been marked.

as obtained from *ab initio* calculations, turn out to be the weakly coupled 2D model and the weakly coupled 1D chains, respectively. The considered spin models, therefore are given as follows:

$$\begin{aligned}
 H^{\text{pristine}} &= J_1 \sum_{i=1}^{N_1} \sum_{j=1}^{N_2} \sum_{k=1}^{N_3} S_{i,j,k} \cdot (S_{i+1,j,k} + S_{i,j+1,k}) \\
 &+ J_2 \sum_{i=1}^{N_1} \sum_{j=1}^{N_2} \sum_{k=1}^{N_3} S_{i,j,k} \cdot (S_{i+1,j+1,k} + S_{i+1,j-1,k}) \\
 &+ J_c \sum_{i=1}^{N_1} \sum_{j=1}^{N_2} \sum_{k=1}^{N_3} S_{i,j,k} \cdot S_{i,j,k+1}, \\
 H^{\text{Ti-doped}} &= J'_1 \sum_{i=1}^{N_1} \sum_{j=1}^{N_2/2} \sum_{k=1}^{N_3} S_{i,2j,k} \cdot S_{i+1,2j,k} \\
 &+ J'_1 t' \sum_{i=1}^{N_1/2} \sum_{j=1}^{N_2/2} \sum_{k=1}^{N_3} S_{i',2j,k} \cdot S_{i',2j\pm 1,k} \\
 &+ J'_c \sum_{i=1}^{N_1/2} \sum_{j=1}^{N_2/2} \sum_{k=1}^{N_3} S_{i',2j,k} \cdot S_{i',2j,k+1} \\
 &[i' = 2i - \text{mod}(k, 2)],
 \end{aligned}$$

where  $J$ 's are the exchange integrals of the spin models as shown in Fig. 7. The above models have been solved by the quantum Monte Carlo method (stochastic series expansion<sup>33</sup>) on a  $14 \times 14 \times 14$  lattice. The QMC computed susceptibility given by  $\chi^{\text{th}} = \langle (S^z - \langle S^z \rangle)^2 \rangle$  is compared with the experimentally measured susceptibility<sup>18</sup> of the pristine compound in the presence of magnetic field of 10 000 Oe via  $\chi = 0.375 S(S+1) \left(\frac{g^2}{J_1}\right) \chi^{\text{th}}$ , at intermediate and high temperature. To simulate the low-temperature behavior we also include curie contribution from impurities as  $\chi^{\text{CW}} = C_{\text{imp}}/T$ . The best fit to experimentally measured susceptibility was obtained for

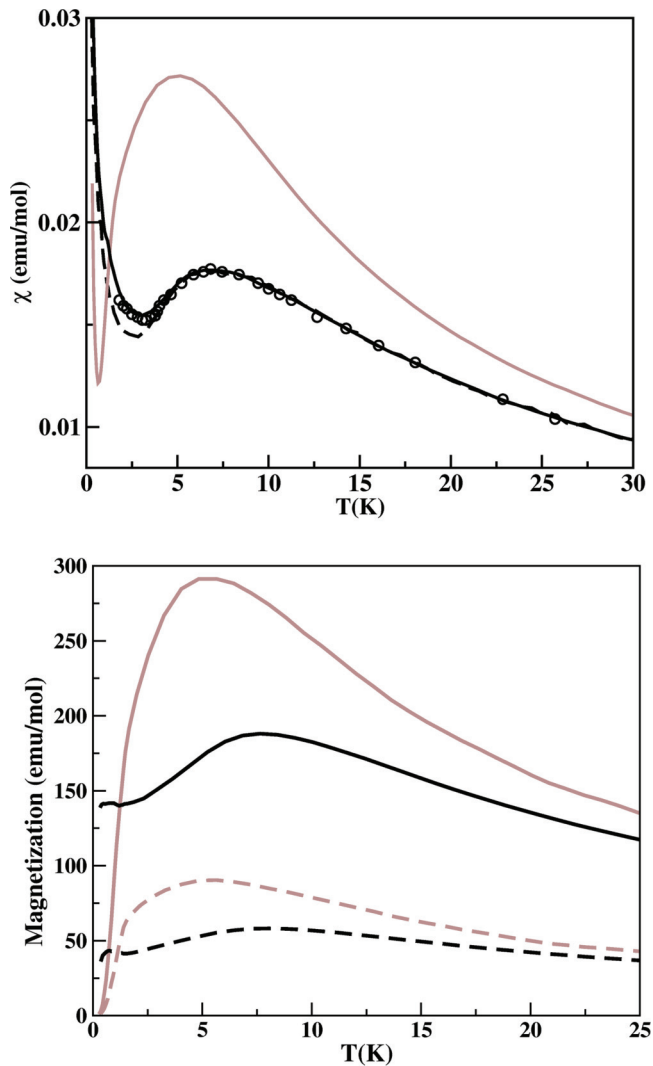


FIG. 8. (Color online) (Upper panel) Calculated magnetic susceptibility plotted as a function of temperature for the pristine (black lines) and Ti-substituted (gray lines) compounds. The magnetic susceptibility for the pristine compound has been computed in the absence (dashed line) and in the presence of applied magnetic field of 10 000 Oe (solid line). The latter has been compared with the experimentally measured data,<sup>18</sup> shown as open circles. (Lower panel) Magnetization plotted as a function of temperature for the pristine (black lines) and Ti-substituted (gray lines) compounds for two different values of the magnetic field,  $H = 5000$  Oe (solid line) and  $H = 1560$  Oe (dashed line).

$g = 2.26$ ,  $J_1 = 8$  K (the ratios  $\frac{J_2}{J_1}$  and  $\frac{J_3}{J_1}$  was fixed at DFT estimates, 0.02 and  $-0.03$ , respectively), and  $C_{\text{imp}} = 0.006$ . In the upper panel of Fig. 8, we show the computed susceptibility for the pristine compound in the presence and absence of magnetic field, comparing with the experimental data obtained in the presence of magnetic field 10 000 Oe. The computed susceptibility for the Ti-substituted model is also presented, which shows drastic changes in behavior compared to the pristine compound. The susceptibility following the presence of a broad maxima, shows an exponential drop at lower temperature signaling the characteristic opening of spin gap. The change in magnetic behavior of the pristine to Ti-substituted compound is also evident in the computed magnetization as a function of temperature for magnetic field strengths, 5000 Oe and 1560 Oe, as shown in the bottom panel of Fig. 8. This undoubtedly shows the control of the magnetic ground state of a typical 2D AFM square lattice through chemical substitution by changing the ground state from a long-ranged ordered one for the pristine compound to a spin-gapped one for the substituted compound. The computed thermodynamic quantities are expected to provide the useful database to check the validity of our predictions through future experimental measurements.

## VI. CONCLUSION

The analysis of the electronic structure of the  $\text{Zn}_2\text{VO}(\text{PO}_4)_2$  compound through first-principles DFT calculations and subsequent calculation of thermodynamics properties by the QMC method, confirms the description of  $\text{Zn}_2\text{VO}(\text{PO}_4)_2$  as the weakly coupled 2D AFM  $S = \frac{1}{2}$  Heisenberg system as predicted earlier by experimental data. Motivated by literature<sup>22</sup> on the effect of spin dilution in destabilizing the long-range order in the 2D AFM lattice, we designed on computer the Ti-substituted  $\text{Zn}_8\text{TiV}_3\text{O}_4(\text{PO}_4)_8$  compound. Our theoretical study predicts the  $\text{Zn}_8\text{TiV}_3\text{O}_4(\text{PO}_4)_8$  compound to be a spin-gapped system, given by a spin model of a weakly interacting 1D spin chain. Our predictions may be verified in terms of future experimental measurements with our computed thermodynamic properties on  $\text{Zn}_8\text{TiV}_3\text{O}_4(\text{PO}_4)_8$ .

## ACKNOWLEDGMENT

The authors thank the Department of Science and Technology, India for support through the Thematic Unit of Excellence and the Unit for Nanoscience and Technology.

<sup>1</sup>P. Lemmens, G. Guntherodt, and C. Gros, *Phys. Rep.* **375**, 1 (2003).

<sup>2</sup>D. A. Tennant, S. E. Nagler, A. W. Garrett, T. Barnes, and C. C. Torardi, *Phys. Rev. Lett.* **78**, 4998 (1997).

<sup>3</sup>D. C. Johnston, J. W. Johnson, D. P. Goshorn, and A. J. Jacobson, *Phys. Rev. B* **35**, 219 (1987).

<sup>4</sup>S. Sarkar, S. Kanungo, and T. Saha-Dasgupta, *Phys. Rev. B* **82**, 235122 (2010); A. A. Tsirlin, A. Möller, B. Lorenz, Y. Skourski, and H. Rosner, *ibid.* **85**, 014401 (2012); O. Janson, A. A. Tsirlin, J. Sichelschmidt, Y. Skourski, F. Weickert, and H. Rosner, *ibid.* **83**, 094435 (2011).

<sup>5</sup>T. Giamarchi, Ch. Regg, and O. Tchernyshyov, *Nature Physics* **4**, 198 (2008)

<sup>6</sup>M. B. Stone, C. Broholm, D. H. Reich, O. Tchernyshyov, P. Vorderwisch, and N. Harrison, *Phys. Rev. Lett.* **96**, 257203 (2006).

<sup>7</sup>A. Zheludev, V. O. Garlea, T. Masuda, H. Manaka, L.-P. Regnault, E. Ressouche, B. Grenier, J.-H. Chung, Y. Qiu, K. Habicht, K. Kiefer, and M. Boehm, *Phys. Rev. B* **76**, 054450 (2007).

<sup>8</sup>B. Leuenberger, H. U. Gdel, and J. K. Kjems, *J. Mag. Mag. Matt.* **53**, 175 (1985).

- <sup>9</sup>Ch. Ruegg, B. Normand, M. Matsumoto, A. Furrer, D. F. McMorrow, K. W. Kramer, H.-U. Gudel, S. Gvasaliya, H. Mutka, and M. Boehm, *Phys. Rev. Lett.* **100**, 205701 (2008).
- <sup>10</sup>H. Tanaka, K. Goto, M. Fujisawa, T. Ono, and Y. Uwatoko, *Physica B: Condensed Matter B* **329-333**, 697 (2003).
- <sup>11</sup>T. Hong, V. O. Garlea, A. Zheludev, J. A. Fernandez-Baca, H. Manaka, S. Chang, J. B. Leao, and S. J. Poulton, *Phys. Rev. B* **78**, 224409 (2008).
- <sup>12</sup>T. Masuda, A. Fujioka, Y. Uchiyama, I. Tsukada, and K. Uchinokura, *Phys. Rev. Lett.* **80**, 4566 (1998).
- <sup>13</sup>L. P. Regnault, J. P. Renard, G. Dhalle, and A. Revcolevschi, *Europhys. Lett.* **32**, 579 (1995).
- <sup>14</sup>Y. Sasago, N. Koide, K. Uchinokura, M. C. Martin, M. Hase, K. Hirota, and G. Shirane, *Phys. Rev. B* **54**, R6835 (1996).
- <sup>15</sup>M. C. Martin, M. Hase, K. Hirota, G. Shirane, Y. Sasago, N. Koide, and K. Uchinokura, *Phys. Rev. B* **56**, 3173 (1997).
- <sup>16</sup>T. Masuda, I. Tsukada, K. Uchinokura, Y. J. Wang, V. Kiryukhin, and R. J. Birgeneau, *Phys. Rev. B* **61**, 4103 (2000).
- <sup>17</sup>T. Waki, Y. Itoh, C. Michioka, K. Yoshimura, and M. Kato, *Phys. Rev. B* **73**, 064419 (2006).
- <sup>18</sup>N. S. Kini, E. E. Kaul, and C. Geibel, *J. Phys.: Condens. Matter* **18**, 1303 (2006).
- <sup>19</sup>S. M. Yusuf, A. K. Bera, N. S. Kini, I. Mirebeau, and S. Petit, *Phys. Rev. B* **82**, 094412 (2010).
- <sup>20</sup>E. Dagotto and T. M. Rice, *Science* **271**, 618 (1996).
- <sup>21</sup>C. Zeng and V. Elser, *Phys. Rev. B* **42**, 8436 (1990).
- <sup>22</sup>S. Taniguchi, Y. Nishikawa, Y. Yasui, Y. Kobayashi, M. Sato, T. Nishikawa, M. Kontani, and K. J. Sano, *Phys. Soc. Jpn.* **64**, 2758 (1995).
- <sup>23</sup>O. K. Andersen and O. Jepsen, *Phys. Rev. B* **12**, 3060 (1975).
- <sup>24</sup>O. K. Andersen and T. Saha-Dasgupta, *Phys. Rev. B* **62**, R16219 (2000).
- <sup>25</sup>O. K. Andersen and O. Jepsen, *Phys. Rev. Lett.* **53**, 2571 (1984).
- <sup>26</sup>G. Kresse and J. Hafner, *Phys. Rev. B* **47**, R558 (1993); G. Kresse and J. Furthmuller, *ibid.* **54**, 11169 (1996).
- <sup>27</sup>J. P. Perdew, K. Burke, and M. Ernzerhof, *Phys. Rev. Lett.* **77**, 3865 (1996).
- <sup>28</sup>V. I. Anisimov, I. V. Solovyev, M. A. Korotin, M. T. Czyzyk, and G. A. Sawatzky, *Phys. Rev. B* **48**, 16929 (1993).
- <sup>29</sup>K. H. Lii and H. J. Tsai, *J. Solid State Chem.* **90**, 291 (1991).
- <sup>30</sup>The defined cell is the conventional unit cell and not the standard unit cell, which are rotated with respect to each other.
- <sup>31</sup>A. W. Garrett, S. E. Nagler, D. A. Tennant, B. C. Sales, and T. Barnes, *Phys. Rev. Lett.* **79**, 745 (1997).
- <sup>32</sup>R. Valenti, T. Saha-Dasgupta, J. V. Alvarez, K. Pozgajcic, and C. Gros, *Phys. Rev. Lett.* **86**, 5381 (2001); T. Saha-Dasgupta, R. Valenti, F. Capraro, and C. Gros, *ibid.* **95**, 107201 (2005); H. Das, T. Saha-Dasgupta, C. Gros, and R. Valenti, *Phys. Rev. B* **77**, 224437 (2008); M. Pregelj, H. O. Jeschke, H. Feldner, R. Valenti, A. Honecker, T. Saha-Dasgupta, H. Das, S. Yoshii, T. Morioka, H. Nojiri, H. Berger, A. Zorko, O. Zaharko, and D. Aron, *ibid.* **86**, 054402 (2012); M. Reehuis, T. Saha-Dasgupta, D. Orosel, J. Nuss, B. Rahaman, B. Keimer, O. K. Andersen, and M. Jansen, *ibid.* **85**, 115118 (2012).
- <sup>33</sup>A. W. Sandvik, *Phys. Rev. B* **59**, R14157 (1999); A. Dorneich and M. Troyer, *Phys. Rev. E* **64**, 066701 (2001); K. Louis and C. Gros, *Phys. Rev. B* **70**, 100410(R) (2004).